J. Phys. D: Appl. Phys. **41** (2008) 015406 (5pp) doi:10.1088/0022-3727/41/1/015406

Morphology transformation of patterned, uniform and faceted GaN microcrystals

Tae Woong Kim[1], Young Joon Hong[2], Gyu-Chul Yi[2], Ji-Hwan Kwon[1], Miyoung Kim[1], Heung Nam Han[1], Do Hyun Kim[1], Kyu Hwan Oh[1], Ki-jeong Kong[3] and Young-Kyun Kwon[4]

[1] Department of Materials Science and Engineering, Seoul National University, Shillim-Dong, Kwanak-Gu, Seoul 151-74, Korea
[2] National CRI Center for Semiconductor Nanorods and Department of Materials Science and Engineering, POSTECH, San-31 Hyoja-dong, Pohang, Gyeongbuk 790-784, Korea
[3] Korea Research Institute of Chemical Technology, PO Box 107, Yuseong, Daejeon 305-600, Korea
[4] Department of Physics and Applied Physics, University of Massachusetts Lowell, One University Avenue, Lowell, MA 01854, USA

E-mail: mkim@snu.ac.kr

Received 4 October 2007, in final form 12 November 2007
Published 19 December 2007
Online at stacks.iop.org/JPhysD/41/015406

Abstract
We report on the growth and characterization of patterned and uniformly distributed GaN microcrystals with well-defined facets and epitaxy. The microcrystals were grown on a mask patterned by lithography. The GaN microcrystals were formed by selective-area epitaxy using metal-organic chemical-vapour deposition. The GaN microcrystals have similar sizes and shapes. Each microcrystal consists of an upper and a lower part, which are rotated by 30°. Transmission electron microscopy shows that there is a rather clear interface between the two parts of the crystal, suggesting a sudden change in the growth direction. We performed *ab initio* calculations for the surface energies of hexagonal GaN, and the growth morphology is explained based on surface energy considerations.

(Some figures in this article are in colour only in the electronic version)

1. Introduction

Advanced techniques have enabled the fabrication and characterization of various nanostructures. Nanostructures with many interesting morphologies have recently been reported [1, 2]. In order to use them in electronic or optical devices, however, it is necessary to control their size and morphology, as well as to obtain a high degree of ordering in terms of their locations, because their properties and functionalities depend on their shape, size, symmetry and long range ordering [3–5]. In this study, we investigate the mechanism of surface morphology transition in GaN microcrystals, and this should be more important for nanostructures which have larger surface to volume ratios. The GaN microcrystals studied in this work are fabricated by catalyst-free metal–organic chemical-vapour deposition (MOCVD), and show an intriguing structural transformation. The observed rotation of the facet planes in the middle of the growth as shown in figure 1, which has not been reported before, entails a strong driving force for the rotation, thus providing a clue to the determination of their morphology.

Morphological or structural transformations during epitaxial growth often occur according to the kinetic growth conditions such as the temperature [6] and pressure [7]. Other interesting morphological transitions include microfaceted nanowires generated by the formation of twin planes [8] and transition from a nanobelt to superlattice-structured nanohelics induced by polar-charge [9]. The growth conditions for the GaN microcrystals in this study remained the same during their growth. We studied their structure using transmission electron microscopy (TEM), and suggest that the morphology transition of selectively grown GaN microcrystals could be explained by the surface energy of GaN.

GaN has a wide band gap and a stable hexagonal structure (space group: $P_6 3mc$, wurtzite) with $a = b = 3.18$ Å, $c = 5.18$ Å, and has many applications in high power/temperature electronics, photonics and spintronics [10, 11]. It can also be grown in the zincblende structure at low temperature.

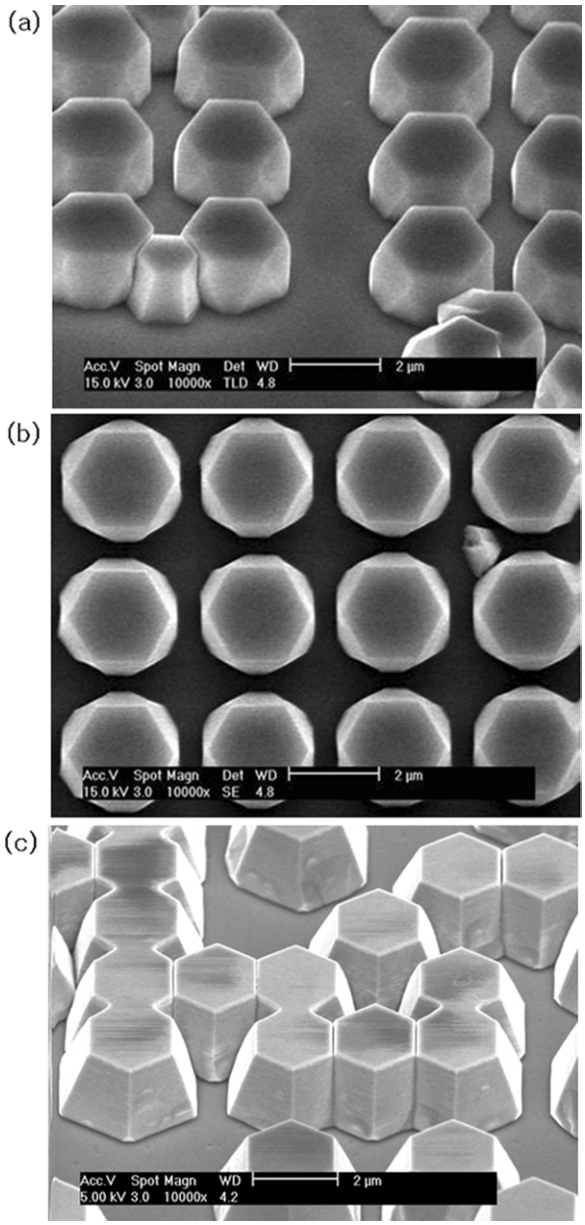

Figure 1. Scanning electron microscopy images of microcrystal arrays with a 3.2 μm interval showing 30° rotation of facets. (*a*) A side view image. (*b*) A top view image; the bottom surface has a dodecagonal shape and the top surface has a hexagonal shape. (*c*) An image of microcrystals without rotation of facets.

The favoured growth direction of wurtzite GaN is the *c*-axis, [0 0 0 1], which results in nonpolar side surfaces. The morphologies of GaN nanostructures have been of great interest [12–14].

2. Experiments

The GaN hexagonal microcrystals studied herein were fabricated on patterned SiO_2/GaN/Al_2O_3 (0 0 0 1) substrates using selective-area MOCVD with a low-pressure (0.3 Torr) vertical reactor-chamber. First, a 1 μm thick GaN seed layer with a 20 nm thick AlN buffer layer was prepared on sapphire using MOCVD at 950 °C, followed by the deposition of a 50 nm thick SiO_2 layer onto the GaN seed layer by plasma-enhanced chemical-vapour deposition. The SiO_2 layer was employed as a growth-mask for the selective growth of GaN micropattern arrays. Then, the SiO_2 layer was coated by PMMA and a dot-array aligned along the [1 0 $\bar{1}$ 0] direction was formed at the desired positions by the e-beam lithographic (EBL) technique (figure 1). The SiO_2 layer in the dot-array was etched by a commercially available buffered oxide etchant (BOE). After lithography, the GaN seed layer which has a diameter of a few hundred nanometres was exposed through the dot-array. While the size and location were determined by the SiO_2 mask, the shape and crystallographic facet of the GaN micropatterns were controlled by adjusting the growth parameters, such as the temperature, pressure, ambient gas, V/III ratio and the pitch of the hole-openings. For the growth of the GaN microcrystal arrays, trimethylgallium (TMGa) and ammonia (99.9995% NH_3) were employed as the reactants, and purified hydrogen was used as a carrier gas. The NH_3 and TMGa flow rates were in the range 5–10 sccm and 10–20 μmol min^{-1}, respectively, and the GaN microcrystal arrays were synthesized at a temperature of 1100 °C.

The morphology and crystal structure of the GaN microcrystals were studied by TEM. The TEM specimens were prepared by a focused ion beam (FIB, Tecnai NOVA 200 nanolab with Omniprobe). Both cross-sectional and plane view specimens were prepared for the TEM observations. A high voltage (1200 kV) transmission electron microscope at the Korea Basic Science Institute (KBSI) was used to obtain the high-resolution images, and a Jeol 3000F was used to obtain the selected area electron diffraction patterns.

3. Results and discussions

3.1. Electron microscopy study

The field-emission scanning electron microscopy (FE-SEM) images in figure 1 show the shape of the GaN microcrystal arrays, in which the facets are rotated by 30° (or equivalently 90°) between the lower (Region I) and upper regions (Region II). The side view in figure 1(*a*) clearly shows the expansion and contraction of the side facet planes as the microcrystal grows. The plane normal to the growth direction at the lower part of a microcrystal is composed of twelve lines, of which the six longer lines increase up to a certain point and then disappear as the microcrystal grows further, while the other shorter six lines form the final hexagonal shape at the top. (See top view image in figure 1(*b*)) The formation of {1 0 $\bar{1}$ 1} and higher index faceted pyramidal hexagonal structures have previously been reported [12], however, the simultaneous rotation of facet planes in the middle of the growth is an unexpected result, especially considering the fact that the growth parameters remained the same throughout the growth process. Typical hexagonal structures without facet rotation are shown in figure 1(*c*) for comparison.

Figure 2 shows a low magnification bright field TEM image of a GaN microcrystal (*a*) and electron diffraction patterns from three different regions, namely, the upper region, the interface and the lower region (b). A thin amorphous

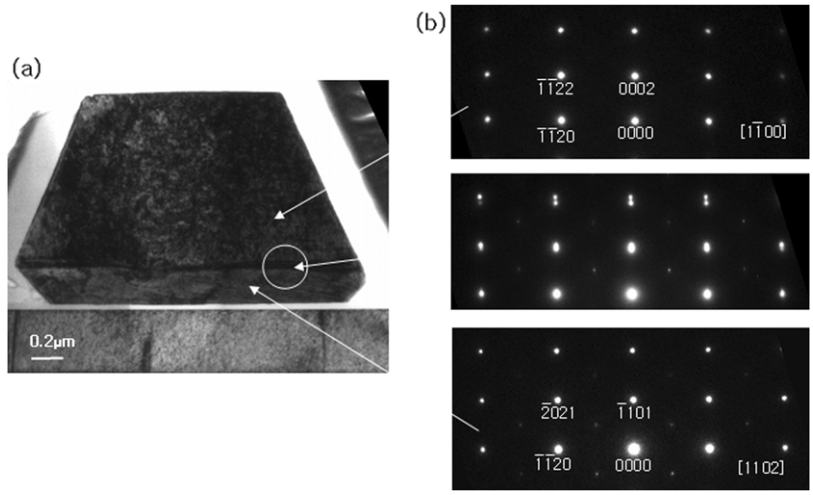

Figure 2. (*a*) Low magnification cross-section TEM image of a microcrystal. (*b*) Electron diffraction patterns taken in the upper (top), the boundary (middle) and the lower (bottom) regions, respectively. The zone axes are [1 $\bar{1}$ 0 0] and [1 $\bar{1}$ 0 2] in the upper and the lower regions.

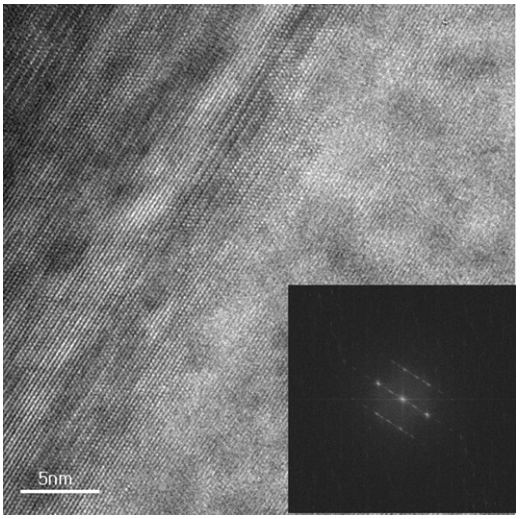

Figure 3. High-resolution images at the boundary between the upper and lower areas. The fast Fourier transform of the micrograph is shown in the inset.

SiO_2 layer between the microcrystal and the substrate is shown in the low magnification image (figure 2(*a*)), which is also confirmed by energy dispersive x-ray spectroscopy (EDS). This unexpected SiO_2 layer, which was supposed to be completely etched, played an important role in the morphology as explained in the last paragraph of this section. The images and diffraction patterns clearly show the existence of two distinctive regions. A high-resolution image at the boundary and its Fourier transformed micrograph are shown in figure 3. The interface region is a few tens of nanometres in size. Many planar dislocations are observed in all the regions, and much more dense dislocations are seen at the boundary region, as shown in the high-resolution image. The fast Fourier transformation (FFT) micrograph of the high-resolution image at the interface between the upper and the lower regions showed strong streaks due to the existence of stacking faults along the growth direction.

The electron diffraction patterns in figure 2(*b*) show that the GaN substrate and the microcrystals grow in the wurtzite structure. The GaN substrate and the upper part of the microcrystal (Region II) have the same growth direction, [0 0 0 1], with a very slight misorientation, less than 3°, between them. The lower part of the microcrystal (Region I) where the dodecagonal shape is formed, on the other hand, grows in the ($\bar{1}$ 1 0 1) orientation. The diffraction pattern taken at the boundary shows the overlapped pattern of the zone axes, [1 $\bar{1}$ 0 0] and slightly off [1 $\bar{1}$ 0 2]. These zone axes of these two regions, [1 $\bar{1}$ 0 0] and [1 $\bar{1}$ 0 2], share the (1 1 $\bar{2}$ 0) planes. It should be mentioned that the lower region (Region I) has weak supercell spots in the diffraction patterns, which disappear as the crystal grows in the [0 0 0 1] direction in the top region. The dark field image of the supercell spots shows that these spots originate from the entire area in the lower part. The size of the supercell structure is doubled along the *c*-axis of the hexagonal unit cell. The presence of ordered vacancies or polarity may cause this supercell structure, but further investigation is needed to explain it.

Figure 4 shows the atomic configurations perpendicular to the growth direction in each area of the microcrystal, (*a*) in the lower region and (*b*) in the upper region. The *x* and *y* directions in figure 4(*a*) are [$\bar{1}$ $\bar{1}$ 2 0] and [1 $\bar{1}$ 0 2], while those in figure 4(*b*) are [$\bar{1}$ $\bar{1}$ 2 0] and [1 $\bar{1}$ 0 0], respectively. The two domains share atoms in the (1 1 $\bar{2}$ 0) planes, and the atomic distances of the Ga atoms in the [1 $\bar{1}$ 0 2] and [1 $\bar{1}$ 0 0] directions differ by about 6%. This lattice mismatch causes dense planar defects at the boundary as shown in the high-resolution image in figure 3. The larger hexagon formed by the intersection of the {1 1 $\bar{2}$ 0} and the {1 0 $\bar{1}$ 2} planes with the ($\bar{1}$ 1 0 1) plane in figure 4(*a*) represents the longer six lines of a dodecagon at the bottom. The smaller hexagon in figure 4(*a*), which is the same as the larger one in figure 4(*b*) made by the intersection of the six {1 1 $\bar{2}$ 0} planes with the (0 0 0 1) plane, is drawn for comparison. This larger hexagon in figure 4(*b*) is gradually replaced by the 30° rotated smaller hexagon in the same figure, formed by the intersection of the six {1 0 $\bar{1}$ 0} planes with the

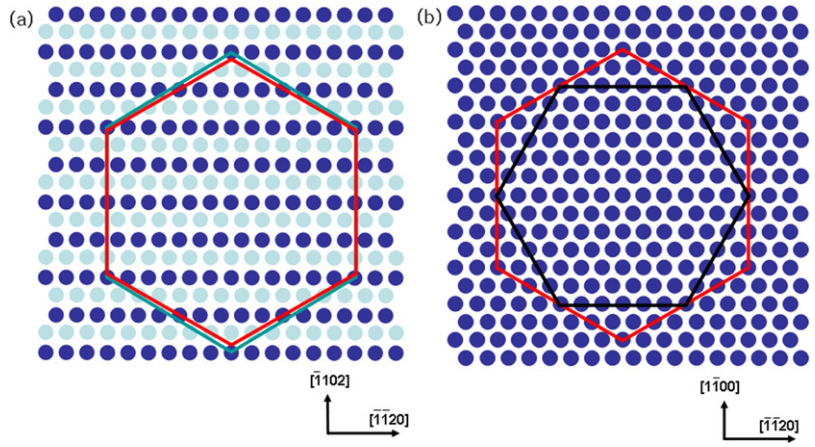

Figure 4. Atomic configurations of the ($\bar{1}$ 1 0 1) surface (*a*) and (0 0 0 1) surface (*b*). The hexagons in the figure represent the lines viewed from the top. Different colours show different atomic layers. The smaller hexagon and the larger hexagon in (*b*) represent lines in the $\{1\,0\,\bar{1}\,0\}$ and $\{1\,1\,\bar{2}\,0\}$ planes, respectively. The inner hexagon in (*a*) is the same as the one in the $\{1\,1\,\bar{2}\,0\}$ planes in (*b*). As the microcrystal grows along the [0 0 0 1] direction in (*b*), the larger hexagon in the $\{1\,1\,\bar{2}\,0\}$ planes becomes smaller and disappear, which makes the smaller hexagon in the $\{1\,0\,\bar{1}\,0\}$ plane at the top area. Thus the morphology of facet rotation is shown.

(0 0 0 1) plane. The smaller hexagon is the final shape at the top surface.

The uncommon initial growth of the lower part may be attributed to the strain between the amorphous SiO_2 and the GaN microcrystals, judging from the fact that the microcrystals are epitaxially grown along the [0 0 0 1] direction from the beginning, thus no rotation of the facet planes occurs when the SiO_2 in the dot-array is etched completely. When the SiO_2 layer is not removed completely, however, the GaN substrate effect on the growth of the GaN microcrystal is reduced, and the kinetic growth condition in the beginning is controlled by the strain between the amorphous SiO_2 layer and the hexagonal GaN. The initial kinetic growth condition controlled by the strain is changed to the near-equilibrium growth conditions corresponding to the fast growth along the [0 0 0 1] direction and, then, the $\{1\,1\,\bar{2}\,0\}$ facets transform into other facets, presumably because of the energy gain due to the difference in the surface energy.

3.2. First-principles calculations

To confirm the qualitative observations described in the previous section, we carried out first-principles calculations of the surface energies of GaN using the Vienna *ab initio* simulation program (VASP) [15, 16]. The calculations were carried out with ultrasoft pseudopotentials [17] using plane waves up to a cutoff energy of 36.8 Ry (500 eV). The exchange-correlation potential is described within the generalized gradient approximation (GGA) [18, 19], and Brillouin-zone integrals were determined through summations over sufficiently dense meshes of special points, at least 30 **k**-points per 1 × 1 surface unit cell. We also performed our calculations using another density functional techinique with the norm-conserving pseudopotential method [20] based on a linear combination of atomic orbitals basis [21, 22] with double-zeta polarization. We also used the GGA for the exchange-correlation potential and an energy cutoff of 200 Ry for the real space mesh. All the surfaces were represented by a periodically repeated symmetric slab consisting of several atomic layers and separated by a vacuum region with thicknesses ranging from 12.9 to 15.3 Å. Slabs with 10–13 atomic layers (containing up to 60 atoms) were used for the $\{1\,1\,\bar{2}\,0\}$ surfaces, and slabs 18–30 atomic layers (also containing up to 60 atoms) were used for the $\{1\,0\,\bar{1}\,0\}$ surface. The surface energies of the planes, $\{1\,0\,\bar{1}\,0\}$ and $\{1\,1\,\bar{2}\,0\}$, are 1.61 J m^{-2} and 1.68 J m^{-2}, respectively. The energy difference between these two planes is 4.2%, which is similar to a previously reported value of 4.7% [23]. Using our first-principles technique, we also calculated the energetics while the dodecagon reduces to the final rotated hexagon. As a GaN microcrystal grows along the [0 0 0 1] direction, the six $\{1\,1\,\bar{2}\,0\}$ planes, which have formed the six longer lines of the dodecagon becoming shorter, disappear and result in six isosceles triangles as shown in figure 1. It turns out that the two congruent sides of the isosceles triangle on the $(1\,1\,\bar{2}\,0)$ plane coincide with the lines along the $[\bar{1}\,1\,0\,1]$ and $[1\,\bar{1}\,0\,1]$ directions, and its corresponding congruent angle is about 62°. Due to the reduction of the $\{1\,1\,\bar{2}\,0\}$ planes by forming these six isosceles triangles, there are six other planes formed in between the two adjacent triangles. Geometrical consideration determines an angle between one of such planes and the base plane of the microcrystal to be about 75.2°. This angle is exactly identical to the angles of the $\{2\,0\,\bar{2}\,1\}$ planes, which become the facets of the microcrystal displayed in figure 1. The growth line of these six $\{2\,0\,\bar{2}\,1\}$ planes, which have originally formed the six shorter lines of the dodecagon, become longer until the $\{1\,1\,\bar{2}\,0\}$ planes disappear completely, forming the final hexagon.

We calculated the energy change during the surface morphology transformation described above. The atomic configurations for the $\{1\,0\,\bar{1}\,0\}$, $\{1\,1\,\bar{2}\,0\}$, and $\{2\,0\,\bar{2}\,1\}$ planes are represented in figure 5. The formation of the six isosceles triangles reduces the surface area of the $\{1\,1\,\bar{2}\,0\}$ planes and increases that of the $\{2\,0\,\bar{2}\,1\}$ planes, which are structurally similar to the $\{1\,0\,\bar{1}\,0\}$ plane. It is calculated that the $\{1\,1\,\bar{2}\,0\}$ planes exhibit a higher surface energy than those of the

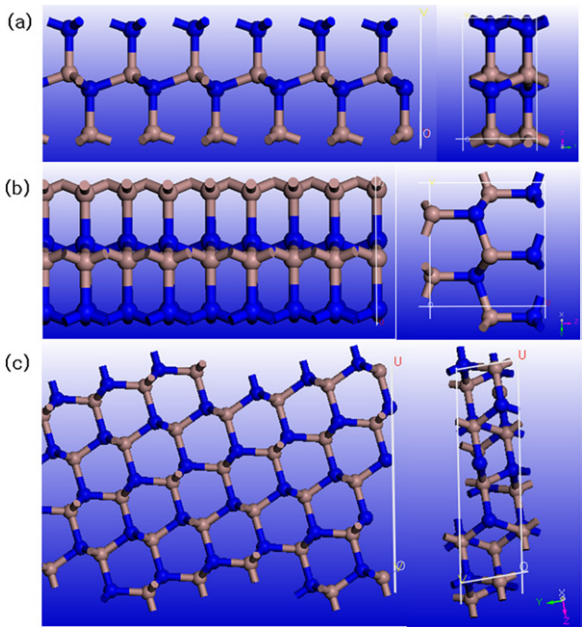

Figure 5. Atomic configurations used for the first-principles calculations. The left figures are side view and the right figures are top view. (*a*) $\{1\,0\,\bar{1}\,0\}$ surface (*b*) $\{1\,1\,\bar{2}\,0\}$ (*c*) $\{2\,0\,\bar{2}\,1\}$ surface.

$\{2\,0\,\bar{2}\,1\}$ planes, 1.67 J m^{-2}, as well as of the $\{1\,0\,\bar{1}\,0\}$ planes. The energy gain due to the morphology change was calculated to be ∼0.11 eV as one layer (∼1.3 Å) grows along the [0 0 0 1] direction. This energy gain is attributed to the reduction of the total surface area and, thus, that of the total surface energy while the GaN microcrystal grows. We believe that this energy gain is large enough to explain the intriguing structural change in the later stage of the GaN microcrystal growth, although a complicated growth kinetics needs to be considered during the earlier stage of the growth.

4. Summary

We fabricated patterned and faceted GaN microcrystals and studied the structural transformation of the selectively grown hexagonal GaN microcrystals using TEM and first-principles calculations. The structural transformation originates from the strain effect and the surface energy anisotropy, that is, the transition of the critical factor in growth from the strain effect to the near-equilibrium condition. The amorphous SiO_2 structure between the substrate and the microcrystal prohibits the epitaxial growth of the (0 0 0 1) GaN microcrystal in the beginning, but after the growth of about 200 nm of $(\bar{1}\,1\,0\,1)$ GaN, fast growth of the (0 0 0 1) orientation is preferred. In this near-equilibrium condition, the energy gain from the surface energy anisotropy causes the rotation of the facets, resulting in the interesting behaviour of facet rotation. This work may be useful for the facet control of nanostructures.

Acknowledgments

The authors thank the Korea Basic Science Institute for the HVEM measurements. This work was supported by grant no R01-2006-000-11071-0 from the Basic Research Program of the Korea Science & Engineering Foundation, and by the Korea Science & Engineering grant funded by the Korean government (MOST) ROA-2007-000-10014-0.

References

[1] Wang Z L, King X Y and Zuo J M 2003 *Phys. Rev. Lett.* **91** 185502
[2] Wiley B J, Xiong Y, Li Z Y, Yin Y and Xia Y 2006 *Nano Lett.* **6** 765
[3] Dalpian G M, Tiago M L, del Puerto M L and Chelikowsky J R 2006 *Nano Lett.* **6** 501
[4] Johansson J, Karlsson L S, Svensson C P T, Martensson T, Wacaser B A, Deppert A, Samuelson A and Seifert W 2006 *Nat. Mater.* **5** 574
[5] Bode M, Pietzsch O, Kubetzka A and Wiesendanger R 2004 *Phys. Rev. Lett.* **92** 067201
[6] Li Z, Sing K, Tok E S, Tan J P Y, Lin M and Foo Y-L 2007 *Appl. Phys. Lett.* **90** 101914
[7] Wang Z, Daemen L L Zhao Y, Zha C S Downs R T Wang X, Wang Z L and Hemley R J 2005 *Nat. Mater.* **4** 922
[8] Habas S E, Lee H, Radmilovic V, Somorjai G A and Yang E 2007 *Nat. Mater.* **6** 692
[9] Gao P X, Ding Y, Mai W, Hughes W L, Lao C and Wang Z L 2005 *Science* **309** 1700
[10] Dietl T, Ohno H, Matsukura F, Cibert J and Ferrand D 2000 *Science* **287** 1019
[11] Nakamura S, Mukai T and Senoh M 1994 *Appl. Phys. Lett.* **64** 1687
[12] Liu H P, Chen I G, Tsay J D, Liu W W, Guo Y D and Hsu J T 2004 *J. Electroceram.* **13** 839
[13] Xiang X, Cao C, Xu Y and Zhu H 2006 *Nanotechnology* **17** 30
[14] Hersee S D, Sun X and Wang X 2006 *Nano Lett.* **6** 1808
[15] Kresse G and Hafner J 1993 *Phys. Rev.* B **47** 558
[16] Kresse G and Furthmueller J 1996 *Phys. Rev.* B **54** 11169
[17] Vanderbilt D 1990 *Phys. Rev.* B **41** 7892
[18] Perdew J P and Wang Y 1992 *Phys. Rev.* B **45** 13244
[19] Perdew J P, Chevary J A, Vosko S H, Jackson K A, Pederson M R, Singh D J and Fiolhais C 1992 *Phys. Rev.* B **46** 6671
[20] Cohen M L 1982 *Phys.Scr.* **T1** 5
[21] Sanchez-Portal D, Ordejon P, Artacho E and Soler J M 1997 *Int. J. Quantum Chem.* **65** 453
[22] Artacho E *et al* 2000 *Phys. Status Solidi* b **217** 335
[23] Northrup J E and Neugebauer J 1996 *Phys. Rev.* B **53** R10477